



HAL
open science

Wide-Speed Range Sensorless Control of Five-Phase PMSM Drive under Healthy and Open Phase Fault Conditions for Aerospace Applications

Ihab Assoun, Lahoucine Idkhajine, Babak Nahid-Mobarakeh, Farid Meibody-Tabar, Eric Monmasson, Nicolas Pacault

► **To cite this version:**

Ihab Assoun, Lahoucine Idkhajine, Babak Nahid-Mobarakeh, Farid Meibody-Tabar, Eric Monmasson, et al.. Wide-Speed Range Sensorless Control of Five-Phase PMSM Drive under Healthy and Open Phase Fault Conditions for Aerospace Applications. *Energies*, 2023, 16 (1), pp.1-18. 10.3390/en16010279 . hal-04159890

HAL Id: hal-04159890

<https://cnam.hal.science/hal-04159890v1>

Submitted on 12 Jul 2023

HAL is a multi-disciplinary open access archive for the deposit and dissemination of scientific research documents, whether they are published or not. The documents may come from teaching and research institutions in France or abroad, or from public or private research centers.


L'archive ouverte pluridisciplinaire **HAL**, est destinée au dépôt et à la diffusion de documents scientifiques de niveau recherche, publiés ou non, émanant des établissements d'enseignement et de recherche français ou étrangers, des laboratoires publics ou privés.



Distributed under a Creative Commons Attribution 4.0 International License

Review

Wide-Speed Range Sensorless Control of Five-Phase PMSM Drive under Healthy and Open Phase Fault Conditions for Aerospace Applications

Ihab Assoun ^{1,2}, Lahoucine Idkhajine ^{1,*} , Babak Nahid-Mobarakeh ³, Farid Meibody-Tabar ⁴, Eric Monmasson ¹  and Nicolas Pacault ²

¹ Laboratory of Systems & Applications of Information & Energy Technologies (SATIE), CY Cergy Paris Université, 95000 Cergy, France

² Aerospace Business Unit, WATT & WELL S.A.S., 91300 Massy, France

³ McMaster Automotive Resource Centre (MARC), McMaster University, Hamilton, ON L8S 4L8, Canada

⁴ Laboratory of Energetics, Theoretical and Applied Mechanics (LEMTA), University of Lorraine, 54000 Nancy, France

* Correspondence: lahoucine.idkhajine@cyu.fr

Abstract: This paper presents a speed sensorless control of a five-phase PMSM in healthy operation and under the Open-Phase Fault on any phase of the machine. The solution is recommended for mission-critical applications requiring high reliability capacities, such as Aerospace applications. An adapted Active Fault Tolerant Control is proposed with the aim of obtaining electromechanical torque as close as possible to that normally developed by a machine working in healthy condition. In instances of a loss of power to one phase of the machine, a reconfiguration of the control law is performed to ensure the continuity of service and to maintain acceptable control performances without requiring a hardware rearrangement of the power architecture. The motor rotation speed and position, required for the Field Oriented Control (FOC) of the stator currents, are estimated using a Back-Electromotive Forces (Back-EMF) observer based on a mathematical model of the motor and implemented in the stator diphasic reference frame. Different electrical models that describe the behavior of the five-phase machine in the normal and degraded operations are given. Experimental results on a 1.25 kW synchronous PM machine are shown to confirm the effectiveness of the motor control.

Keywords: fault tolerant control; motor sensorless control; five-phase PMSM drives; Field Oriented Control; back-EMF; systems reliability



Citation: Assoun, I.; Idkhajine, L.; Nahid-Mobarakeh, B.; Meibody-Tabar, F.; Monmasson, E.; Pacault, N. Wide-Speed Range Sensorless Control of Five-Phase PMSM Drive under Healthy and Open Phase Fault Conditions for Aerospace Applications. *Energies* **2023**, *16*, 279. <https://doi.org/10.3390/en16010279>

Academic Editors: Massimiliano Luna and Marcello Pucci

Received: 11 November 2022

Revised: 10 December 2022

Accepted: 22 December 2022

Published: 27 December 2022



Copyright: © 2022 by the authors. Licensee MDPI, Basel, Switzerland. This article is an open access article distributed under the terms and conditions of the Creative Commons Attribution (CC BY) license (<https://creativecommons.org/licenses/by/4.0/>).

1. Introduction

Reliability is one of the most critical requirements when developing AC drive systems for space applications. While this is true for systems such as satellites, spacecraft, or any other payload systems, it is even more true for the space launch vehicle that puts them into orbit. Indeed, a space launch failure is one of the most expensive losses as these payloads can cost up to several billion dollars. For instance, on the European launcher Ariane 6, which will have its first test flight in the next future, the launch of the load into orbit and the de-orbiting of the second stage of the rocket after its mission are conducted by a thermal engine whose fuels (Oxygen & Hydrogen) must be kept pressurized. This task is ensured by electrical moto-pump AC drives that must be highly reliable and resilient during the entire mission.

To start with, the reliability must be guaranteed by the main element of the electromechanical chain, which is the controlled motor. For this purpose, multi-phase Permanent Magnet Synchronous Machines (PMSM) bring additional degrees of freedom (in addition to power segmentation and torque density), by allowing operating continuity after any

fault occurring on the power supply of one or more phases [1,2]. Such electrical faults are frequently caused by the Voltage Source Inverter (VSI) and, in particular, the power switches (40% of occurrence [3]).

In such instances, Fault Tolerant Controllers (FTC) have to be implemented in order to maintain acceptable operating conditions. These FTC can be structured into two main types: Passive FTC and Active FTC. The first type is known to be faster and less computationally complex, but can only deal with certain faults selected at the design phase [4]. In contrast, an active FTC algorithm, which can handle more types of faults and achieve optimum performance, has the ability to reconfigure itself using the information provided by a Fault Detection and Identification system (FDI). Fault detection in electromagnetic systems is widely investigated [5]. In addition, Ref. [6] presents a comprehensive review of the faults and diagnostic methods for PMSM. Several studies have previously been carried out with the aim of finding good control approaches and suitable inverter topologies to improve the reliability of the drive. For example, [7] is one interesting synthesis in this topic and provides progressive fault diagnosis techniques for PMSM, as well as the latest trends in terms of FTC strategies. One of the first studies to focus on the control of multiphase machines in the case of the loss of one or more phases is [8] who conducted a study that deals with the supply of multiphase PMSM by modular voltage inverters (with Open-End and star-connected windings PMSM). Control strategies are proposed to cancel the torque ripples due to the absence of power to one or more phases of the machine. These strategies are based on the modification of the waveform of the current flowing in one or more healthy stator phases to compensate for the missing currents of the faulty phases. However, the currents are controlled directly in the fixed stator reference frame, using hysteresis regulators, which are not suitable for many applications where noise and vibrations generated by non-fixed switching frequencies are troublesome.

To be able to use an efficient controller for phase currents, some studies have proposed matrices of reference frame transformations to control these currents in the d-q basis. Ref. [9] proposes a new adapted Clarke matrix, which allows the five-phase PMSM electrical variables to be represented in a synchronous rotating reference frame, in instances of an Open-Phase Fault (OPF). The coefficients of the matrix are determined to maintain a total Magneto-Motive Force (MMF) and the back-EMFs are similar to those in normal operation (i.e., rotating and circular). A major advantage of this transformation, compared to those proposed in other papers, is that the inductance matrix in the synchronous frame is diagonal (provided that the homopolar component is zero), which considerably simplifies the equations. Ref. [10] introduces a systematic approach based on the generation of the reference frame change matrix. This approach allows the sinusoidal currents to be retained in the stator frame, without the injection of current harmonics. For a five-phase PMSG, [11] proposed an FTC algorithm based on a Generalized Proportional Integral Observer (GPIO) disturbance observer that acts directly on the internal current control loops of the fundamental and third harmonics current frequencies. The method proposed in this reference seeks to overcome the constraints related to the accuracy of the machine model experienced by other techniques.

In addition to these electrical faults, the mechanical side also has its own negative impact on the system reliability. Indeed, the used rotor position sensor (mandatory for closed-loop Field-Oriented Control) is also subject to failures [1]. Furthermore, in highly critical applications, such as the one presented in this paper, the use of such mechanical sensors is not possible because of rotor shaft accessibility. This is the reason why sensorless control strategies are the unique alternative for reliable and affordable drives. In this way, several solutions have been developed to substitute the hardware feedback sensor, depending on the speed range. For medium and high speeds, one can underline machine model-based techniques, such as the Extended Kalman Filter [12], the Back-EMF estimator [13] and the sliding mode observer [14]. For the lowest speeds and standstill, where the observability is downgraded, methods consisting in tracking the saliency of the rotor, such as the high frequency injection [15] and the transient excitation methods [16], can be used.

In this work, the authors deal with an aerospace application in which both of these electrical and mechanical aspects are combined. This application consists of an oxygen-hydrogen moto-pump that uses a high speed 5-phase PMSM (30 kRPM, 0.396 Nm). To the best of the authors' knowledge, few equivalent works that focus on this particular combination of both electrical and mechanical faults are available in the literature (examples are [17–19]). Additionally, other studies have been interested in this problem for three-phase electrical machines, in which it is necessary to apply a hardware reconfiguration for a post-fault operation [14]. Regarding multiphase machines, some research has been conducted recently to allow for the sensorless control of the five-phase machine in the degraded mode. In [20], a sensorless control strategy based on the Sliding Mode Observer (SMO) for a seven-phase PMSM has been proposed. The harmonic richness of this machine is exploited to implement an observer for each of the significant harmonics (1, 3 and 9). Ref. [21] deals with a particular case in which only one switch on an inverter arm is condemned to the open state and exploits the induced freewheeling current to extract information on the mechanical position.

The main contribution of this work is the development of a highly reliable and online reconfigurable control system that combines both the FTC aspects to prevent any OPF and, at the same time, the sensorless aspects, as there is no embedded position sensor in the mechanical chain. Thus, a Fault Detection and Identification (FDI) algorithm has been developed to detect any arbitrary OPF sequence, which allows an automatic reconfiguration of the implemented PMSM controller of the Back-EMF position/speed estimator. In addition, this paper presents additional functionalities that have been embedded within the controller in order to minimize the impact of critical PMSM harmonics on the torque quality and the estimation quality.

The paper is organized as follows. In the next section, the setup characteristics are presented and models of the five-phase PMSM in different operation conditions are given. Section 3 discusses the developed reconfigurable controller and also explains the proposed harmonic minimization process. In Section 4, a deeper description of the rotor position estimator is made. For each section, the analyses and discussions are fully based on experimental tests and waveforms that are provided. Finally, the conclusions of the study are presented in Section 5.

2. Description of the Developed Application

2.1. PMSM Drive Specifications

The developed AC drive system is presented in Figure 1. The power part consists of a five-phase PMSM, which is designed to operate in a wide speed range (up to 30 kRPM, and 0.396 Nm nominal torque). Additional characteristics of this PMSM are given in the Appendix A. The stator windings are fed by a five-leg half-bridge MOSFET-based inverter. The control system includes a Proportional-Proportional Integral speed regulator [22], a reconfigurable current controller (in order to cover healthy and random OPF conditions), a rotor speed/position Back-EMF based estimator and the FDI block.

The corresponding experimental test bench is shown in Figure 2. A three-phase PMSG, connected to resistors, is coupled to the PMSM shaft in order to emulate the moto-pump fluid load. The DC-link voltage is 55 V and the sampling and switching frequencies are fixed to 40 kHz with a dead-time equal to 500 ns. The overall control has been implemented and tested on a dSpace MicroLabBox platform.

In order to optimize the execution time of the algorithms, while keeping the suitable computational time step (25 μ s), we made use of Multi-Processing (MP) by implementing all of the control algorithms on two processors of the MicroLabBox real time system. The two processors work together synchronously and share the computational load, as shown in Figure 3.

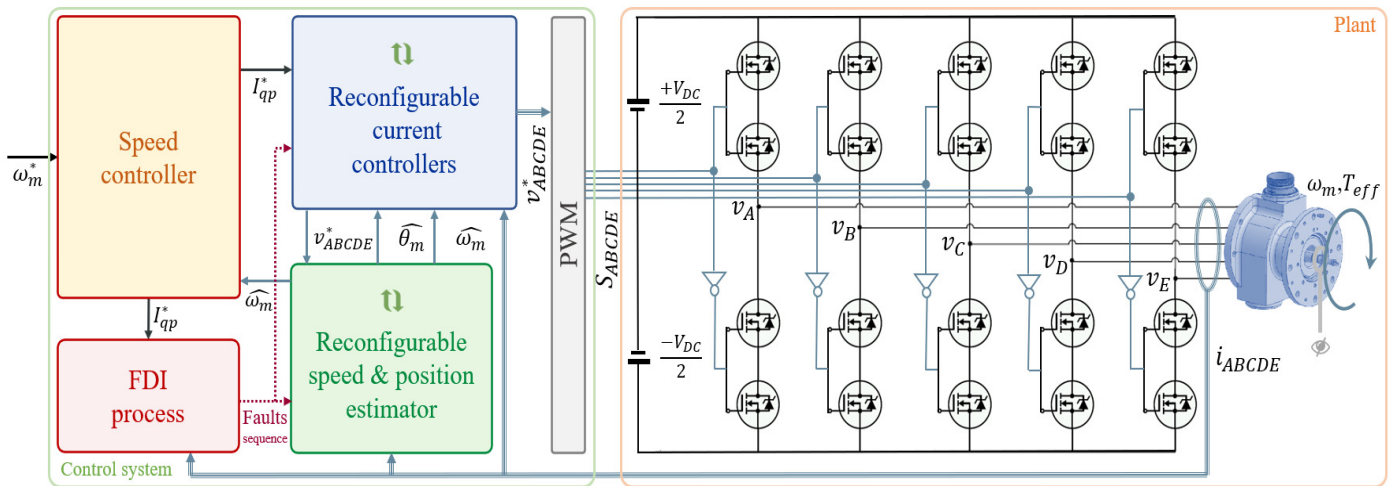


Figure 1. Structure of the developed five-phase PMSM drive system.

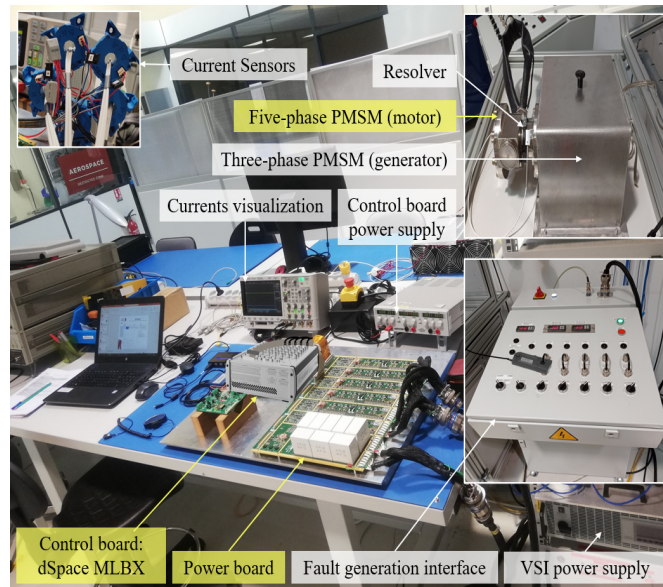


Figure 2. Overview of the experimental test bench.

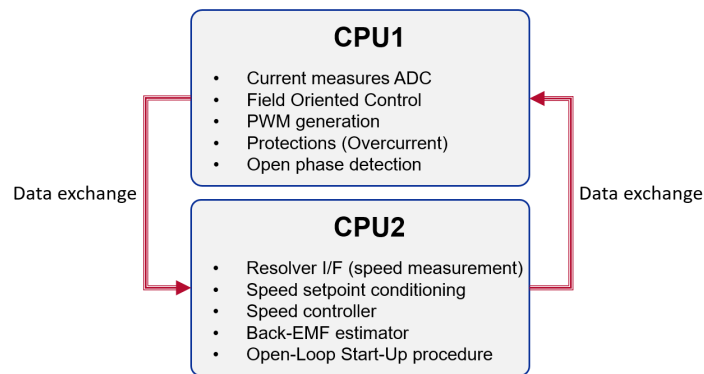


Figure 3. Control implementation on the processors.

When focusing on the PMSM electromagnetic behavior, the experimental Back-EMF waveform and harmonic distribution (for phase A) are given in Figure 4. Although they seem negligible, the fact that the PMSM parameters are very low demonstrates the impact

of these harmonics on the controlled currents waveforms. Consequently, the minimization of this impact through the control algorithm is necessary. More details will be given in Section 3.

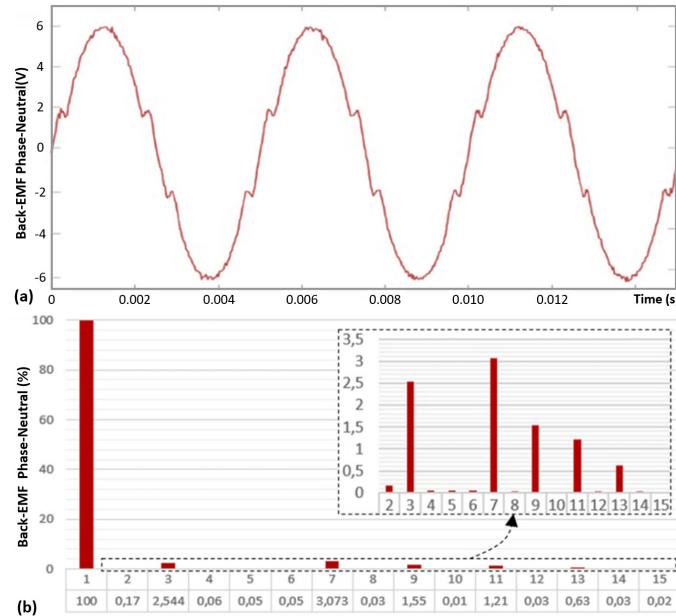


Figure 4. Measured Back-EMF waveform (a) and harmonic distribution (b).

2.2. Five-Phase PMSM Model under Healthy Condition

In a healthy condition, the PMSM (d - q) model can be structured into two fictitious machines: a main machine and a secondary machine. According to the previous harmonic distribution, the main machine (dp - qp) gathers the first and ninth harmonic and the secondary, in turn, gathers the third and seventh harmonics. Equation (1) highlights the corresponding electrical equations and Equation (2) gives the expression of the (d - q) Back-EMF terms.

$$\begin{cases} v_{dp} = R_s \cdot i_{dp} + L_{dp} \cdot di_{dp}/dt - \omega \cdot L_{qp} \cdot i_{qp} + e_{dp} \\ v_{qp} = R_s \cdot i_{qp} + L_{qp} \cdot di_{qp}/dt + \omega \cdot L_{dp} \cdot i_{dp} + e_{qp} \\ v_{ds} = R_s \cdot i_{ds} + L_{ds} \cdot di_{ds}/dt + 3\omega \cdot L_{qs} \cdot i_{qs} + e_{ds} \\ v_{qs} = R_s \cdot i_{qs} + L_{qs} \cdot di_{qs}/dt - 3\omega \cdot L_{ds} \cdot i_{ds} + e_{qs} \end{cases} \quad (1)$$

$$\begin{cases} e_{dp} = -9\Psi_{pm9} \cdot \omega \cdot \sin(10\theta) \\ e_{qp} = \Psi_{pm1} \cdot \omega - 9\Psi_{pm9} \cdot \omega \cdot \cos(10\theta) \\ e_{ds} = -7\Psi_{pm7} \cdot \omega \cdot \sin(10\theta) \\ e_{qs} = -3\Psi_{pm3} \cdot \omega + 7\Psi_{pm7} \cdot \omega \cdot \cos(10\theta) \end{cases} \quad (2)$$

This (d - q) model has been obtained after the $Clarke_F$ and $Park_F$ frame transformations (in healthy mode) illustrated in Equations (3)–(5), where $\delta = 2\pi/5$ denotes the spatial angular shift between consecutive phases. As for the electromagnetic torque, Equation (6) gives the corresponding expression assuming that i_{dp} , i_{ds} and i_{qs} are perfectly regulated to zero.

$$\begin{bmatrix} i_{dp} & i_{qp} & i_{ds} & i_{qs} & i_h \end{bmatrix}^T = [T_{Park_H}] \cdot \begin{bmatrix} i_{\alpha p} & i_{\beta p} & i_{\alpha s} & i_{\beta s} & i_h \end{bmatrix}^T = [T_{Park_H}] \cdot [T_{Clarke_H}] \cdot \begin{bmatrix} i_A & i_B & i_C & i_D & i_E \end{bmatrix}^T \quad (3)$$

$$[T_{Clarke_H}] = \frac{2}{5} \cdot \begin{bmatrix} 1 & \cos(\delta) & \cos(2\delta) & \cos(3\delta) & \cos(4\delta) \\ 0 & \sin(\delta) & \sin(2\delta) & \sin(3\delta) & \sin(4\delta) \\ 1 & \cos(2\delta) & \cos(\delta) & \cos(\delta) & \cos(2\delta) \\ 0 & \sin(2\delta) & \sin(-\delta) & \sin(\delta) & \sin(-2\delta) \\ 1 & 1 & 1 & 1 & 1 \end{bmatrix} \quad (4)$$

$$[T_{Park_H}] = \begin{bmatrix} \cos\theta & \sin\theta & 0 & 0 & 0 \\ -\sin\theta & \cos\theta & 0 & 0 & 0 \\ 0 & 0 & \cos3\theta & -\sin3\theta & 0 \\ 0 & 0 & \sin3\theta & \cos3\theta & 0 \\ 0 & 0 & 0 & 0 & 1 \end{bmatrix} \tag{5}$$

$$T_{em} = \frac{5}{2} \cdot p \cdot i_{qp} [\Psi_{pm1} - 9 \cdot \Psi_{pm9} \cdot \cos(10\theta)] \tag{6}$$

2.3. Five-Phase PMSM Model under OPF Condition

To start with, let us assume that an OPF appears in the phase A of the PMSM. In this case, a new model is mandatory to describe the behavior of the new non-symmetrical four-phase machine. In the literature, several approaches have been suggested with different coordinate transformations [9,10,23]. The approach developed in [9] has been adopted in the proposed work. A major advantage of this transformation, compared to those proposed in other papers, is that the inductance matrix in the synchronous frame remains diagonal (assuming that the homopolar component is zero), which considerably simplifies the size of the model equations and the tuning of the regulators.

The corresponding *ClarkeF* and *ParkF* frame transformations are given as follows:

$$\begin{aligned} [i_{dp} \ i_{qp} \ i_z \ i_h]^T &= [T_{Park_F}] \cdot [i_{\alpha p} \ i_{\beta p} \ i_z \ i_h]^T \\ &= [T_{Park_F}] \cdot [T_{Clarke_F}] \cdot [i_B \ i_C \ i_D \ i_E]^T \end{aligned} \tag{7}$$

$$[T_{Clarke_F}] = \frac{2}{5} \begin{bmatrix} \cos(\delta) - 1 & \cos(2\delta) - 1 & \cos(2\delta) - 1 & \cos(\delta) - 1 \\ \sin(\delta) & \sin(2\delta) & -\sin(2\delta) & -\sin(\delta) \\ -\sin(2\delta) & \sin(\delta) & -\sin(\delta) & \sin(2\delta) \\ 1 & 1 & 1 & 1 \end{bmatrix} \tag{8}$$

$$[T_{Park_F}] = \begin{bmatrix} \cos\theta & \sin\theta & 0 & 0 \\ -\sin\theta & \cos\theta & 0 & 0 \\ 0 & 0 & 1 & 0 \\ 0 & 0 & 0 & 1 \end{bmatrix} \tag{9}$$

This transformation includes only the main machine. It can be assumed that, in faulty cases, the secondary machine is neglected. The third and fourth line of the *ClarkeF* matrix are, respectively, linked to an additional z-axis, which is orthogonal to the *dp* and *qp* axes, and to the homopolar axis h. Its major advantage, compared to those proposed in other papers, is that the inductance matrix in the synchronous frame remains diagonal (assuming that the homopolar component is zero), which considerably simplifies the size of the model equations and the tuning of the regulators.

From this transformation, the new OPF machine model (loss of phase A) can be expressed as shown in Equation (10). As for the electromagnetic torque, the corresponding expression is given in Equation (12), knowing that *ih* = 0 (neutral point not connected) and assuming that *idp* and *iz* are regulated to 0.

$$\begin{cases} v_{dp} = R_s \cdot i_{dp} + L_{dp} \cdot di_{dp}/dt - \omega \cdot L_{qp} \cdot i_{qp} + e_{dp} \\ v_{qp} = R_s \cdot i_{qp} + L_{qp} \cdot di_{qp}/dt + \omega \cdot L_{dp} \cdot i_{dp} + e_{qp} \\ v_z = R_s \cdot i_z + L_z \cdot di_z/dt + e_z \\ v_h = e_h \end{cases} \tag{10}$$

$$\begin{cases} e_{dp} = -9\Psi_{pm9} \cdot \omega \cdot \sin(10\theta) \\ e_{qp} = \Psi_{pm1} \cdot \omega - 9\Psi_{pm9} \cdot \omega \cdot \cos(10\theta) \\ e_z = 3\Psi_{pm3} \cdot \omega \cdot \cos(3\theta) - 7\Psi_{pm7} \cdot \omega \cdot \cos(7\theta) \\ e_h = 2/5 \cdot \Psi_{pm1} \cdot \omega \cdot \sin(\theta) + 2/5 \cdot 3\Psi_{pm3} \cdot \omega \cdot \sin(3\theta) \\ \quad + 2/5 \cdot 7\Psi_{pm7} \cdot \omega \cdot \sin(7\theta) + 2/5 \cdot 9\Psi_{pm9} \cdot \omega \cdot \sin(9\theta) \end{cases} \tag{11}$$

$$\begin{aligned}
 T_{em} = & (5/2) \cdot p \cdot i_{qp} \cdot [\Psi_{pm1} \\
 & - (1/2) \cdot 3\Psi_{pm3} \cdot (\cos(2\theta) - \cos(4\theta)) \\
 & - (25/8) \cdot 7\Psi_{pm7} \cdot (\cos(6\theta) - \cos(8\theta)) \\
 & - (1/8) \cdot 9\Psi_{pm9} \cdot (21\cos(8\theta) - 13\cos(10\theta))]
 \end{aligned}
 \tag{12}$$

2.4. Generalization of PMSM Model to Arbitrary Phase Loss

Thus far, we have dealt with the case where the open phase fault occurs on a specific phase, namely the A phase of the machine. The starting point to generalize the faulty model to any phase loss is to assume that all the phases are balanced and supplied by identical VSI legs. In addition, the probability of failure occurring in the power switches is assumed to be the same for the overall VSI topology. It is also worth noting that this work only addresses the case of one phase loss.

Then, the first step is to rearrange the input vector of the $Clarke_F$ transformation depending on the lost phase. As illustrated in Figure 5, the first element of this vector is the phase located next to the faulty one, and the other elements are updated in a circulating way.

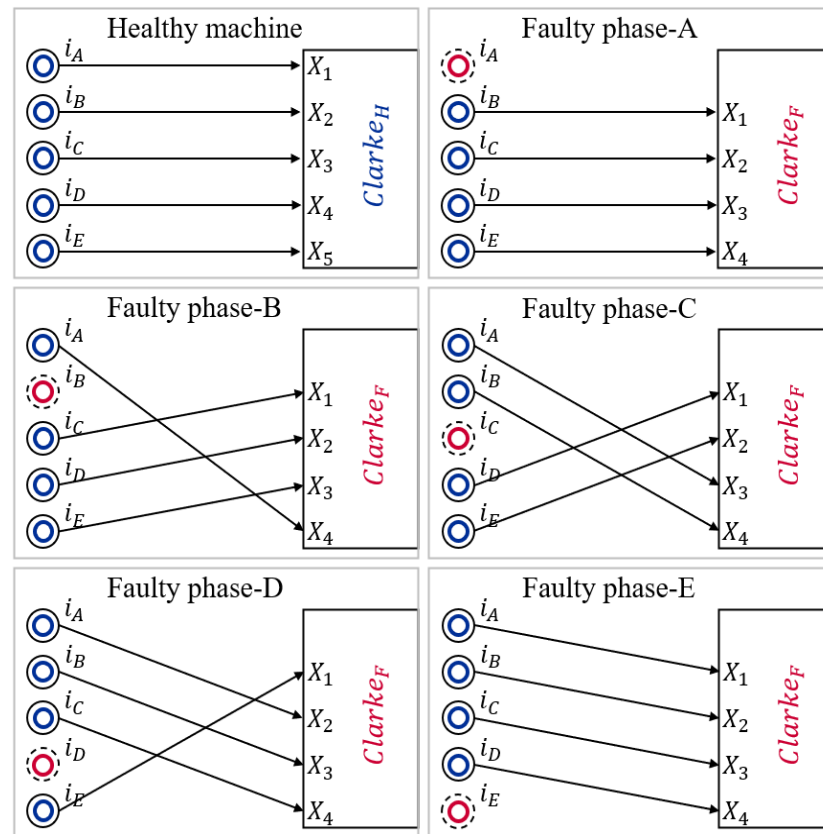


Figure 5. Updating of the input vector of the Clarke transformation depending on the OPF situation.

By making this rearrangement, the same $Clarke_F$ matrix (Equation (8)) can be used. However, the obtained stationary (α - β) currents will be shifted over the first elements of the input vector (first phase) and the value of this shift depends on the number lost phase (n_{FP}). Figure 6 highlights the values of this shift, which has to be compensated through the $Park_F$ transformation, according to the following equation:

$$\hat{\theta} = \hat{\theta}_{phA} - [\delta(n_{FP} - 1) + \theta_x]
 \tag{13}$$

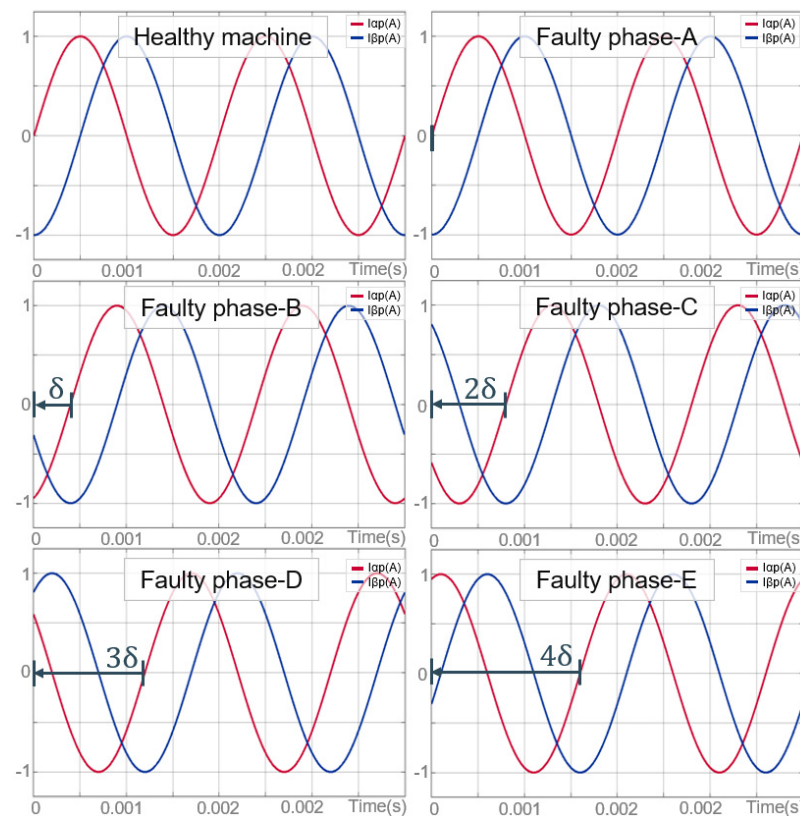


Figure 6. Waveforms of the Clarke transforms outputs in different phase loss conditions.

3. Reconfigurable Fault Tolerant Control

After developing models that describe the behavior of the machine in the healthy mode and when a stator phase is open, the objective is to design a reconfigurable Fault Tolerant controller that allows the overall system to operate in a healthy condition, as well as in the presence of an OPF on a random machine phase. Depending on the condition of the stator phases, the algorithm should commute automatically between two control strategies, while considering the generalization of the fault management on all phases.

3.1. Description of the Reconfigurable Current Controller

Figure 7 provides a general overview of the developed reconfigurable current controller. The first stage includes the healthy and generalized faulty frame transformations (resp. H and F indices), which generate the d - q vectors (selected depending on the fault situation using multiplexers, $fault = 0$ in healthy mode and $fault = 1$ in faulty mode). Then, five PI regulators are implemented in order to regulate the primary (p index) and secondary (s index) d - q components of the machine. The decoupling of the axes, the compensation of the Back-EMF, and the harmonic compensation (see next sub-section) are made afterwards. Finally, the reconfigurable reverse frame transformations are executed to generate the five-phase references that are transferred to the PWM process.

The current reference i_{qp}^* is generated by the speed controller and i_{dp}^* is set to zero. The secondary machine current references (i_{ds}^* , i_{qs}^*) are also set to zero, meaning that the third current harmonic is regulated to zero. In faulty operation, imposing a zero current reference for the z -axis current ($i_z^* = 0$) results in four phase currents of equal amplitude in pairs. In the literature, this strategy is called MJL (Minimal Joule Losses) [10].

The speed controller is designed according to [22] and consists of two nested loops. The inner loop is based on a proportional (P) controller and aims to impose the poles of the system at the desired location. The external loop is based on a PI controller and provides the

desired static and dynamic responses. The speed controller’s architecture and coefficients remain unchanged under all operating conditions.

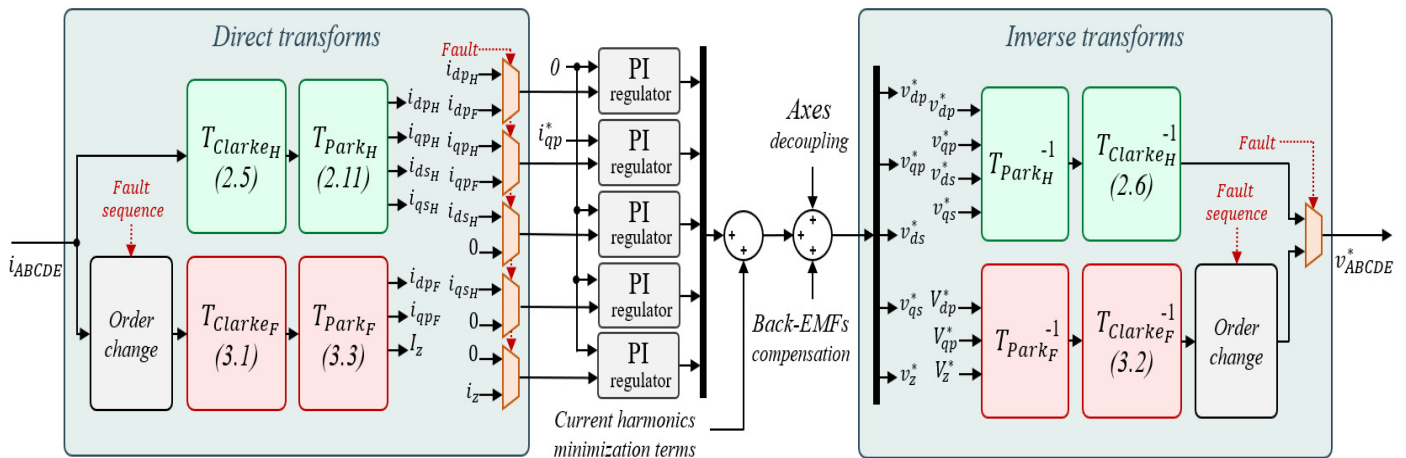


Figure 7. Overview of the reconfigurable current controller.

Regarding the fault detection, the developed FDI process is based on the observation of the phase current measurements. When the current value in a machine phase falls below a fixed threshold for a certain amount of time, the phase is considered as opened. This detection time depends on the speed. After the detection of the opening of a phase is validated, the switches of the corresponding inverter arm are opened.

3.2. Minimization of the Harmonics Impact on the Current Control

During the experimental validations, it was observed that the seventh (in healthy mode) and the second harmonics (in faulty mode) have significant amplitudes that downgrade the quality of the current waveforms. Consequently, their minimization is necessary, and the main idea is to use PI-regulators to set their amplitudes to zero. Figure 8 shows the corresponding block diagram.

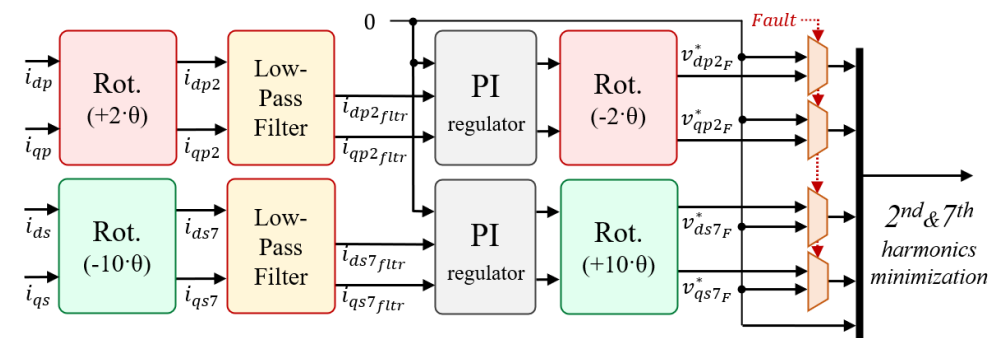


Figure 8. Harmonics minimization mechanism.

Regarding the seventh harmonic, the corresponding amplitude can be extracted by applying a negative $(-10 \cdot \hat{\theta})$ rotation of the secondary (ids, iqs) currents. Then, after a low-pass filtering, these constant values can be controlled to zero by PI regulators. The outputs of the latter are in turn rotated back (with $+10 \cdot \hat{\theta}$) and the obtained voltages (v_{ds7h}^*, v_{qs7h}^*) are injected within the secondary voltage references through multiplexers and in healthy condition ($fault = 0$).

The same principle is applied to the second harmonic: first a positive rotation $(+2 \cdot \hat{\theta})$, low-pass filtering, PI-regulators and then a negative $(-2 \cdot \hat{\theta})$ rotation. The obtained voltage

references are injected within the main voltage references through multiplexers in a faulty condition ($fault = 1$).

3.3. Experimental Validation of the Reconfigurable FTC Algorithm

The following subsection presents the obtained experimental results in order to demonstrate the importance of the implementation of the FTC control. These results are obtained using the rotor position and speed provided by the Back-EMF estimator (Section 4). To start with, Figures 9–11 highlight the obtained experimental results for three situations: a healthy mode, the loss of phase A but without control reconfiguration and the loss of phase A with a control reconfiguration. For all of these tests the current reference i_{qp}^* has been set to 25A.

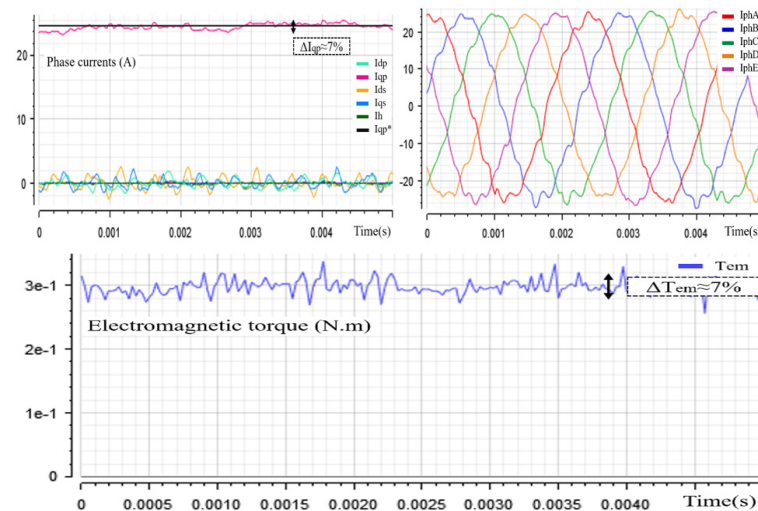


Figure 9. Stator currents and electromagnetic torque in Healthy condition.

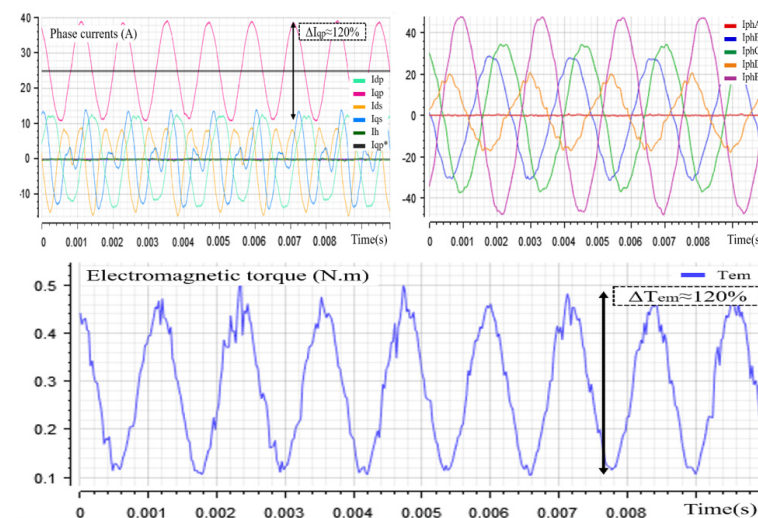


Figure 10. Stator currents and electromagnetic torque in Faulty condition.

Under healthy operation, it can be underlined that the measured i_{qp} is well regulated and the observed oscillations are maintained inside a 7% margin. In the faulty condition (i.e., Under an OPF without reconfiguration), the control is completely downgraded and unacceptable oscillations on the ($d-q$) currents are observed. Consequently, the maximum current values of some of the phases reach high levels (more than twice their normal value). In addition, the torque undulation rate reaches high values that can be considered dangerous (around 120% for this operation point). Finally, after having applied the

proposed FTC strategy, the machine behavior has been considerably improved. The currents and torque oscillations have been reduced to acceptable oscillations margin (16% for electromagnetic torque).

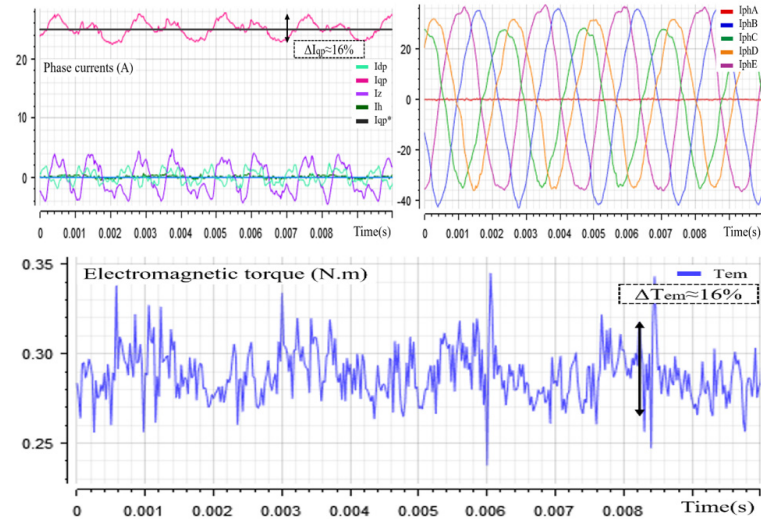


Figure 11. Stator currents and electromagnetic torque in Reconfigured operation.

Figure 12 presents the waveforms of the stator currents before and after the loss of the phase A at time 12.215 s. The detection of the open phase is based on the continuous monitoring of the stator currents. To each measured current, a current threshold proportional to i_{qp}^* and a time-window depending on the electrical period are associated. If the modulus of the current falls below the set threshold for a period longer than the defined window, the phase is considered open. The FDI process takes around 30% of a fundamental electrical period to detect and reconfigure the controller. During this relative time-window, an overshoot of 33% has been observed in the rotating i_{qp} current, as seen in Figure 13.

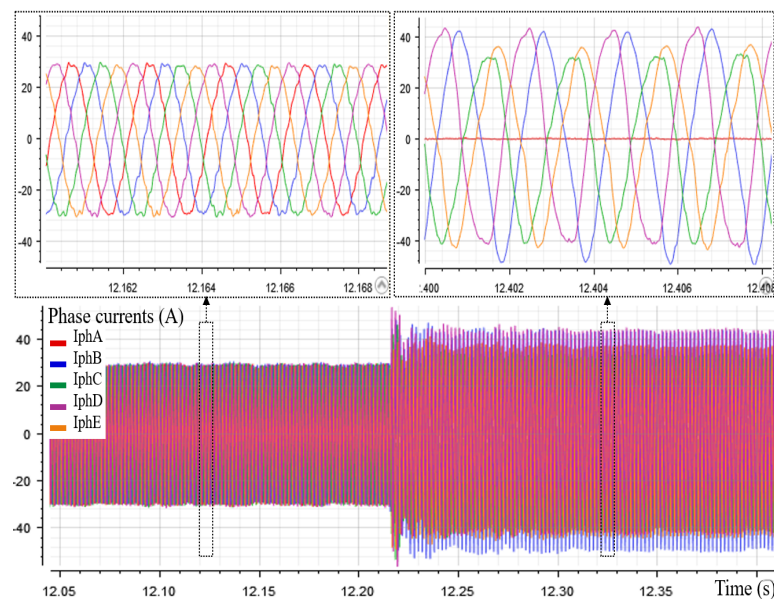


Figure 12. Phase currents before and after the fault on phase A.

Before the fault occurrence, the amplitude is set to 29.3A (speed reference equal to 30 kRPM). After the OPF, to achieve the same operating point (29.3A, 30 kRPM), the adopted MJL strategy imposes 37.12A to the C-E phases and 42.86A to the B-D phases [8]. The

oscillations of the current i_{qp} and the electromagnetic torque (Figure 14) have been limited to an acceptable oscillation margin ($\Delta I_{qp} = 19.38\%$ and $\Delta t_{em} = 20.4\%$ versus $\Delta I_{qp} = 4.9\%$ and $\Delta t_{em} = 7.2\%$ in healthy control). The same successful results have been obtained for arbitrary phase loss and Figure 15 gives the waveforms corresponding to each case.

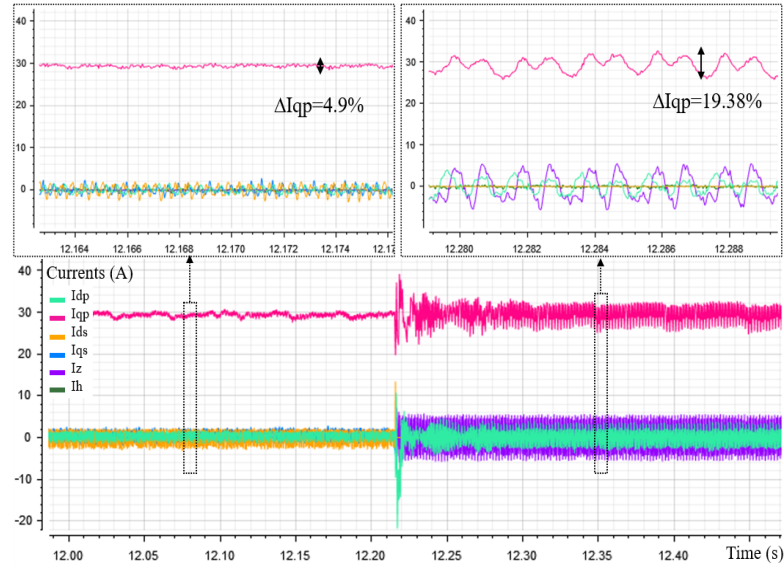


Figure 13. DQ currents before and after the fault on phase A.

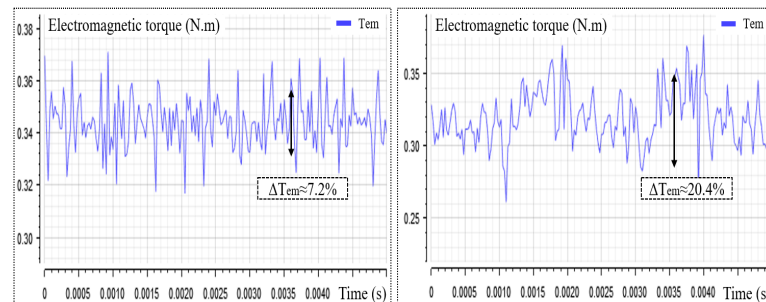


Figure 14. Electromagnetic torque waveforms.

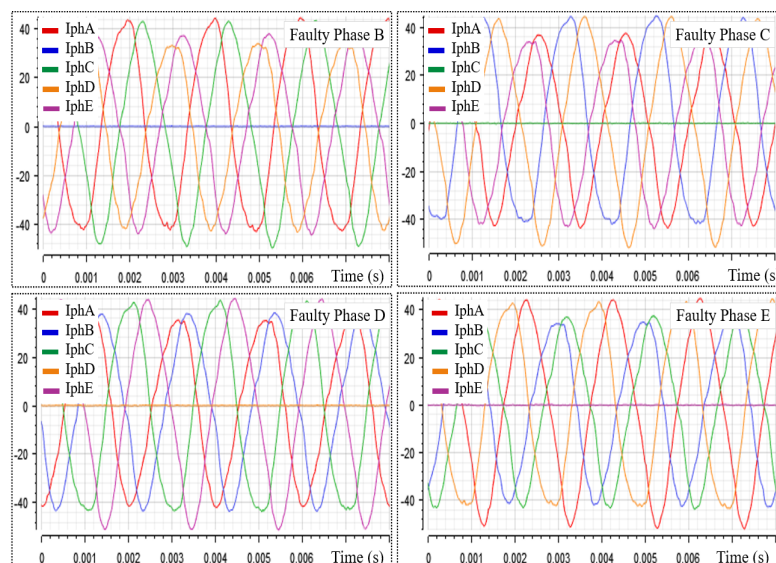


Figure 15. FTC current waveforms.

Furthermore, all these results have been obtained assuming that the second and seventh harmonics are minimized. Figure 16 highlights the case of the seventh harmonic in a healthy condition. It can be clearly seen that the post-filtered amplitude is minimized, resulting in a better quality of the stator currents waveforms. The same positive behavior is highlighted in Figure 17 pertaining to the second harmonic minimization under the OPF condition.

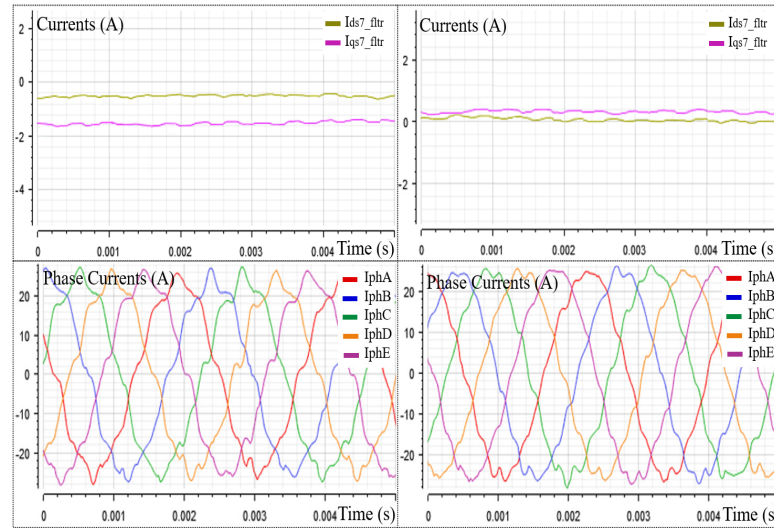


Figure 16. Minimization of the 7th harmonic impact in healthy condition: before (left) and after (right), 25A-25600RPM operating point.

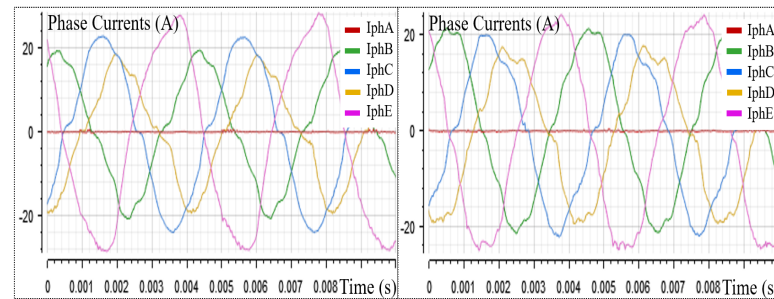


Figure 17. Minimization of the 2nd harmonic impact in healthy condition: before (left) and after (right), 25A-25600RPM operating point.

4. Reconfigurable Back-EMF Sensorless Estimator

As mentioned earlier, the reliability constraints of the developed aerospace application do not allow the use of a mechanical sensor. Consequently, this makes the implementation of a position and speed estimator mandatory and the adopted sensorless method is based on the PMSM Back-EMF.

4.1. Back-EMF-Based Estimation Algorithm

Figure 18 presents the overall synoptic of the developed estimator. The Back-EMF vector is predicted by using the two first equations of the PMSM electrical model in the $(\alpha-\beta)$ frame (Equation (3)), but considering only the fundamental harmonic, as expressed in Equation (14).

$$\begin{cases} \hat{e}_{\alpha p}(t) = v_{\alpha p}^*(t) - R_s \cdot i_{\alpha p}(t) - L_{\alpha p} \cdot di_{\alpha p}/dt \\ \hat{e}_{\beta p}(t) = v_{\beta p}^*(t) - R_s \cdot i_{\beta p}(t) - L_{\beta p} \cdot di_{\beta p}/dt \end{cases} \quad (14)$$

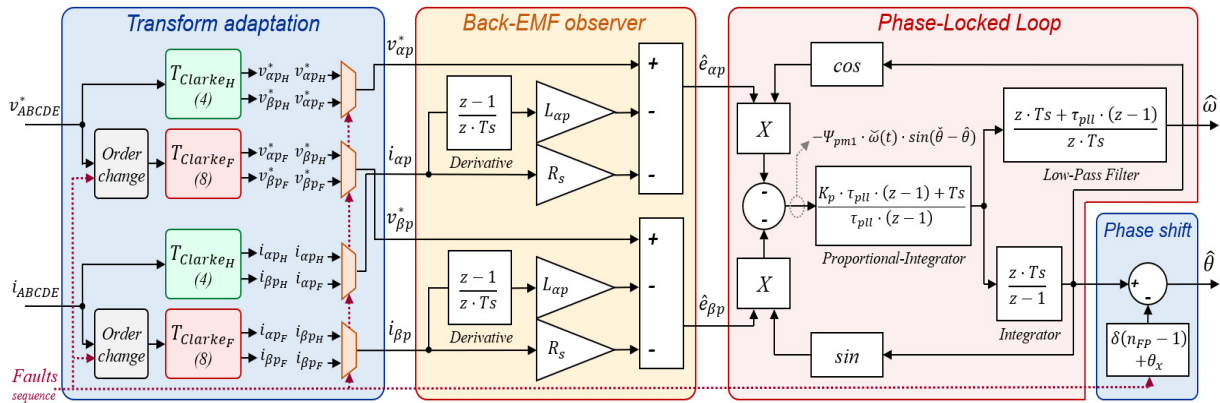


Figure 18. Synoptic of the Back-EMF-based estimator.

Instead of using measured stator voltages, those provided by the controller (v_{ABCDE}^*) are directly used. Furthermore, to consider all of the operating conditions (healthy and arbitrary OPF), the same reconfigurable Clarke transformations shown in Figure 7 are used.

The extraction of the rotor speed and position is then achieved using a Phase-Locked-Loop (PLL) process. The parameters of the internal PI compensator have been tuned experimentally to have an adequate bandwidth (in our case: $K_p = 1.15 \times 10^3$ and $\tau_{PLL} = 1.0$ ms). As a recall, the sampling time step is synchronized with the PWM and set to 25 μ s. The mechanical position is calculated from the estimated speed by integration.

4.2. Experimental Validation of the Back-EMF Based Sensorless Control

Figure 19 highlights the evolution of the estimated and measured speeds with regards to the speed controller reference. This is a full sensorless test as the estimated quantities are injected to the control closed-loop. The measured data (provided by a resolver mounted in the motor shaft) are only used for comparison purposes. One can notice a negligible estimation error since its maximum amplitude (3.36%) appears at the instant 12.215 s, corresponding to the loss of one phase. Even after this fault, the estimation and the sensorless control qualities are still convenient and in a very large speed range (from 100% down to 3.3% of the nominal speed). Regarding the standstill and very-low speed, an open-loop start-up procedure of the PMSM has been developed. This short phase consists of imposing a rotation angle and controlling the phase currents with a progressive speed increase.

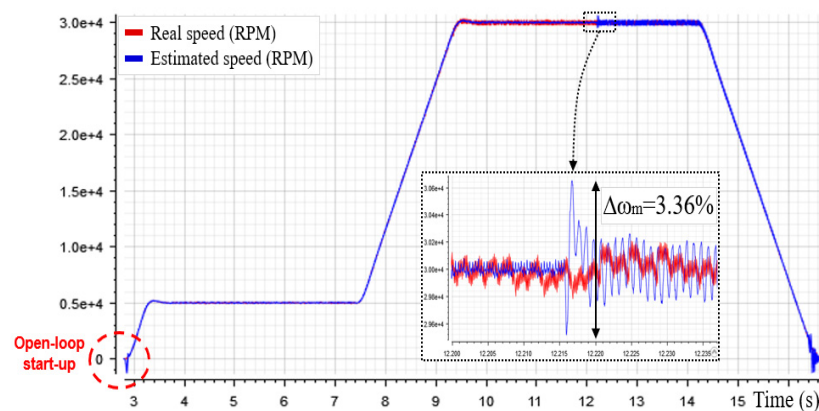


Figure 19. Waveforms of rotor real and estimated speed.

Thanks to the adopted reconfigurable Clark transformation, the estimated Back-EMFs in the (α - β) frame have similar shapes in both the healthy and OPF modes, which is

confirmed in Figure 20. The observed noise on the curves is primarily caused by the current measurement and this noise will be filtered by the bandwidth of the PLL.

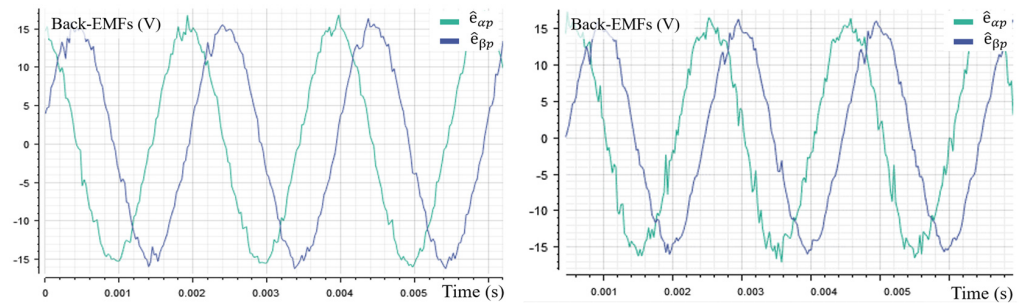


Figure 20. Back-EMFs estimates at maximum speed: Healthy (left) under OPF (right).

Furthermore, the electrical model considered for the estimation of the BEMFs does not demonstrate a considerable dependence on the values of the stator resistances and inductances, since, as can be seen in Table A1, these have very small values. The voltage drops of the windings are negligible compared to the voltage induced by the rotation.

Figure 21 shows the estimated rotor position compared to its measured counterpart for different speeds. The left side concerns the healthy condition, and the right side concerns the case of losing the phase A. A very good tracking of the actual angle is achieved, and the maximum estimation error observed does not exceed 6.3° (1.75%), which is very acceptable for the sensorless control.

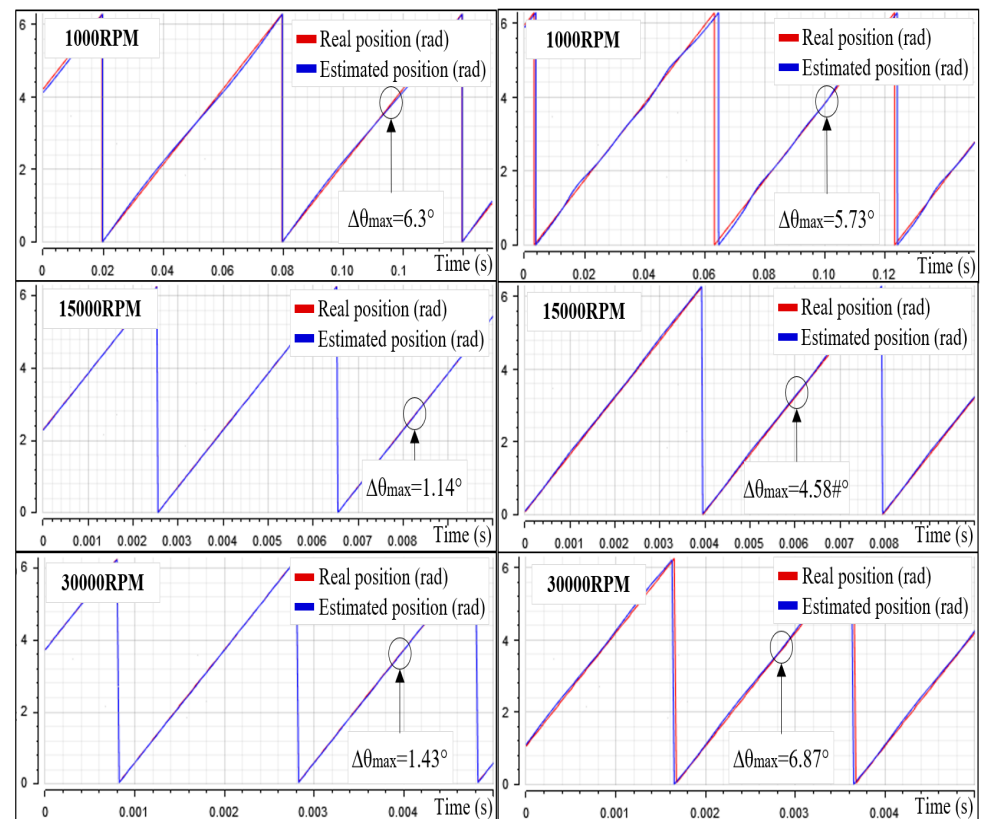


Figure 21. Rotor position estimates in healthy (left) and Open phase A (right) conditions for different speeds.

5. Conclusions

In this paper, we have presented a position sensorless control combined with a fault tolerant control algorithm of a high-speed pole PMSM made for an aerospace application. The use of both techniques increases the reliability of the drive system, allowing both the tolerance to an open electrical phase and the elimination of the mechanical sensor. The performance of the control system is experimentally evaluated at relatively low, medium, and high speeds. The position/speed estimation converges over a wide range of frequencies, providing the sensorless control of the machine between 3% and 100% of the maximum speed in the different operating scenarios studied. In cases of a loss of power to a machine winding, a reconfiguration of the current controllers and the position estimator is performed. The motor torque ripples are strongly minimized in the degraded operation compared to the faulty operation. The technique can be extended to two open phase faults, as long as the transformation matrices provide the same inputs to the position estimator as in healthy control.

Funding: This work was supported by WATT & WELL company (Aerospace and defense BU) and the French Ministry of Higher Education, Research, and Innovation under the CIFRE program.

Data Availability Statement: Not available.

Conflicts of Interest: The authors declare no conflict of interest.

Nomenclature

v	Stator winding phase-neutral voltage (V)
i	Stator winding current (A)
e	Back-Electromotive force (V)
R_s	Stator winding phase-neutral resistance (Ω)
L	Stator winding phase-neutral inductance (H)
ω	Rotor electrical speed (rad/s)
θ	Rotor electrical position (rad)
δ	Angular shift between consecutive phases = $2\pi/5$
T_{em}	Electromagnetic torque (N.m)
Ψ_{pmx}	Permanent Magnet Back-EMF constant (V/(rad/s))
T_{Clarke}	Clarke reference frame transform matrix
T_{Park}	Park reference frame transform matrix
p	Number of pole pairs
n_{FP}	Number of the stator faulty phase

Indexes

H	Healthy condition related variable
F	Faulty condition related variable
p	Primary fictitious machine related variable
s	Secondary fictitious machine related variable
m	Mechanical variable
$ABCDE$	Stator fixed five-phase reference frame variables
α, β	Stator fixed two-phase reference frame variables
d, q	Rotor rotating two-phase reference frame variables
z	Additional axis variables in faulty condition
h	Homopolar axis variables
*	Setpoint variable
$\hat{}$	Estimated variable

Appendix A

Table A1. PMSM characteristics.

Symbol	Quantity	Value	Unit
-	Winding coupling	Starpoint	-
p	Number of pole pairs	1	-
R_s	Winding resistance (PH-N)	9.25×10^{-3}	Ω
L_0	Winding self-inductance	2.64×10^{-5}	H
M_{12}	Consecutives phases mutual	0.193×10^{-5}	H
M_{13}	Non-consecutives phases mutual	-1.43×10^{-5}	H

References

- Betin, F.; Capolino, G.A.; Casadei, D.; Kawkabani, B.; Bojoi, R.I.; Harnefors, L.; Levi, E.; Parsa, L.; Fahimi, B. Trends in Electrical Machines Control: Samples for Classical, Sensorless, and Fault-Tolerant Techniques. *IEEE Ind. Electron. Mag.* **2014**, *8*, 43–55. [[CrossRef](#)]
- Priestley, M.; Farshadnia, M.; Fletcher, J.E. FOC Transformation for Single Open-Phase Faults in the Five-Phase Open-End Winding Topology. *IEEE Trans. Ind. Electron.* **2020**, *67*, 842–851. [[CrossRef](#)]
- Yang, S.; Bryant, A.; Mawby, P.; Xiang, D.; Ran, L.; Tavner, P. An industry-based survey of reliability in power electronic converters. In Proceedings of the 2009 IEEE Energy Conversion Congress and Exposition, San Jose, CA, USA, 20–24 September 2009; pp. 3151–3157.
- Amin, A.A.; Hasan, K.M. A review of Fault Tolerant Control Systems: Advancements and applications. *Measurement* **2019**, *143*, 58–68. [[CrossRef](#)]
- Zhang, W.; Wang, Z.; Li, X. Blockchain-based decentralized federated transfer learning methodology for collaborative machinery fault diagnosis. *Reliab. Eng. Syst. Saf.* **2023**, *229*, 108885. [[CrossRef](#)]
- Chen, Y.; Liang, S.; Li, W.; Liang, H.; Wang, C. Faults and Diagnosis Methods of Permanent Magnet Synchronous Motors: A Review. *Appl. Sci.* **2019**, *9*, 2116. [[CrossRef](#)]
- Li, R.; Wu, Z.; Li, X. Review on fault diagnosis and active fault tolerant control of permanent magnet synchronous motor drive system. *J. Appl. Sci. Eng.* **2021**, *24*, 185–205. [[CrossRef](#)]
- Martin, J.P. Contribution à L'alimentation en Tension de Machines Synchrones à Aimants Permanents à Nombre de Phases Elevé: Fonctionnement Normal et Dégradé. Ph.D. Thesis, Lorraine INP, Vandœuvre-lès-Nancy, France, July 2003.
- Tian, B.; Mirzaeva, G.; An, Q.; Sun, L.; Semenov, D. Fault-Tolerant Control of a Five-Phase Permanent Magnet Synchronous Motor for Industry Applications. *IEEE Trans. Ind. Appl.* **2018**, *54*, 3943–3952. [[CrossRef](#)]
- Seck, A.; Moreau, L.; Benkhoris, M.; Machmoum, M. Automatic generation of optimal phase currents for five-phase PMSG control under open phase condition. In Proceedings of the IECON 2017—43rd Annual Conference of the IEEE Industrial Electronics Society, Beijing, China, 29 October–1 November 2017; pp. 3847–3852.
- Zhuo, L.I.U. Real-Time Fault Diagnosis and Fault-Tolerant Control of 5-Phase Non-Sinusoidal Back-EMF PMSG-Based Tidal Turbine Systems. Ph.D. Thesis, Université de Nantes, Nantes, France, December 2021.
- Idkhajine, L.; Monmasson, E.; Maaalouf, A. Fully FPGA-based sensorless control for synchronous AC drive using an extended Kalman filter. *IEEE Trans. Ind. Electron.* **2012**, *59*, 3908–3915. [[CrossRef](#)]
- Nahid-Mobarakeh, B.; Meibody-Tabar, F.; Sargos, F. Back-EMF estimation based sensorless control of PMSM: Robustness with respect to measurement errors and inverter irregularities. In Proceedings of the Conference Record of the 2004 IEEE Industry Applications Conference, 2004, 39th IAS Annual Meeting, Seattle, WA, USA, 3–7 October 2004; Volume 3, pp. 1858–1865.
- Maamouri, R. Diagnostic et Commande Tolérante Aux Défauts Appliqués à Un Système de Conversion Electromécanique à Base D'une Machine Asynchrone Triphasée. Automatique. Ph.D. Thesis, Ecole Centrale Marseille; Ecole Nationale d'Ingénieurs de Sousse-ENISO (Tunisie), Sousse, Tunisia, 2017. (In Français).
- Zine, W.; Makni, Z.; Monmasson, E.; Chen, K.; Idkhajine, L.; Condamine, B. Hybrid position estimator based on high-frequency signal injection and machine learning for EV fault-tolerant control. In Proceedings of the IECON 2017—43rd Annual Conference of the IEEE Industrial Electronics Society, Beijing, China, 29 October–1 November 2017; pp. 4627–4632.
- Landsmann, P.; Kennel, R. Saliency-based sensorless predictive torque control with reduced torque ripple. *IEEE Trans. Ind. Appl.* **2012**, *27*, 4311–4320. [[CrossRef](#)]
- Furmanik, M.; Scelba, G.; Rafajdus, P. Fault-Tolerant Sensorless Control for Six-Phase PMSM with Dual Back-EMF Observer. In Proceedings of the 2022 International Symposium on Power Electronics, Electrical Drives, Automation and Motion (SPEEDAM), Sorrento, Italy, 22–24 June 2022; pp. 305–311. [[CrossRef](#)]
- Saleh, K.; Sumner, M. Sensorless Control of a Fault Tolerant Multi-level Inverter PMSM Drives in Case of an Open Circuit Fault. In Proceedings of the 2018 International Symposium on Power Electronics, Electrical Drives, Automation and Motion (SPEEDAM), Amalfi, Italy, 20–22 June 2018; pp. 883–888. [[CrossRef](#)]

19. Qiu, X.; Ji, J.; Zhou, D.; Zhao, W.; Chen, Y.; Huang, L. A Modified Flux Observer for Sensorless Direct Torque Control of Dual Three-Phase PMSM Considering Open-Circuit Fault. *IEEE Trans. Power Electron.* **2022**, *37*, 15356–15369. [[CrossRef](#)]
20. Mini, Y. Développement D’algorithmes pour le Contrôle sans Capteur de Machines Electriques Polyphasées en Mode Normal et Dégradé”. Sciences de L’ingénieur (Physics). Ph.D. Thesis, HESAM, Paris, France, 2021. (In French).
21. Tian, B.; Molinas, M.; An, Q.; Zhou, B.; Wei, J. Freewheeling Current-Based Sensorless Field-Oriented Control of Five-Phase Permanent Magnet Synchronous Motors Under Insulated Gate Bipolar Transistor Failures of a Single Phase. *IEEE Trans. Ind. Electron.* **2021**, *69*, 213–224. [[CrossRef](#)]
22. Naouar, M.W.; Naassani, A.; Monmasson, E.; Slama-Belkhdja, I. FPGA based speed control of synchronous machine using a P–PI controller. In Proceedings of the IEEE International Symposium on Industrial Electronics, Montreal, QC, Canada, 9–13 July 2006; pp. 1527–1532.
23. Cheng, L.; Sui, Y.; Zheng, P.; Wang, P.; Wu, F. Implementation of Postfault Decoupling Vector Control and Mitigation of Current Ripple for Five-Phase Fault-Tolerant PM Machine Under Single-Phase Open-Circuit Fault. *IEEE Trans. Power Electron.* **2018**, *33*, 8623–8636. [[CrossRef](#)]

Disclaimer/Publisher’s Note: The statements, opinions and data contained in all publications are solely those of the individual author(s) and contributor(s) and not of MDPI and/or the editor(s). MDPI and/or the editor(s) disclaim responsibility for any injury to people or property resulting from any ideas, methods, instructions or products referred to in the content.